2D Winding losses calculation for round conductor coil

Luo, Tianming; Niasar, Mohamad Ghaffarian; Vaessen, Peter

DOI
10.1109/TPEL.2022.3230724

Publication date
2022

Document Version
Final published version

Published in
IEEE Transactions on Power Electronics

2-D Winding Losses Calculation for Round Conductor Coil

Tianming Luo, *Student Member, IEEE*, Mohamad Ghaffarian Niasar, and Peter Vaessen, *Member, IEEE*

***Abstract*—Winding loss calculation is essential for inductor and transformer design. In this article, a revised 1-D Ferreira's formula is proposed, which considers the interaction between conductors. Then, a 2-D loss calculation approach is proposed based on the analytical solution of round conductors under a uniform external field. An equivalent external magnetic field is calculated to estimate the winding losses, considering the impact of eddy current. The proposed approach is compared with the 2-D FEM with three types of windings and shows good accuracy with less than 10% error. 3-D FEMs and samples are built based on two simulated windings to validate the loss calculation.**

***Index Terms*—Analytical method, eddy current, losses, skin effect, transformer winding.**

I. Introduction

WINDING losses are essential parts of the losses in magnetic components. With increasing switching frequencies and power ratings of semiconductor devices, inductors and transformers have higher power densities, and the conditions for heat dissipation become worse. Therefore, optimization is necessary for thermal management, and an accurate winding loss estimation is needed. Two general winding loss estimation approaches are the analytical methods and the finite-element model (FEM). The analytical methods are fast but are always limited to certain situations. With FEM, it is possible to obtain losses of any winding configuration with reasonable accuracy. However, a simulation needs to be performed for each configuration, which requires a high computational effort and may be unfriendly to the inexperienced user. Therefore, analytical methods are widely used as the first step of the design.

1-D models, like Dowell's model and Ferreira's formula [1], [2], are developed decades ago. Dowell's model is based on the analysis of foil windings and can be extended to windings with different conductor shapes by converting them to foil windings with equal dc conductance. Ferreira introduced orthogonality into the winding loss calculation and provided the formulas for round conductors based on the Bessel function. The two 1-D methods were compared with 2-D FEM and measurements in several papers [3], [4], [5], [6]. It is shown that Dowell's model has good accuracy for compacted windings. However, Ferreira's formula significantly overestimates the losses of compacted windings and is more suitable for widely-spaced windings. The overestimation was attributed to the neglect of interaction between conductors [7]. Ferreira's formula is adopted for round cross-section Litz wires windings [8], [9], [10], [11], [12], [13], and the formula is supposed to be accurate when the radius is less than 0.8 times skin depth [13]. Dowell's model is also used for rectangular cross-section Litz wire [14]. Various works have tried to improve analytical methods. Whitman [15] analyzed foil windings in cylindrical coordinates. Wojda and Kazimierczuk [16] provide the approximated equations for round conductors based on Dowell's model. Bartoli [17] introduced the porosity factor into Ferreira's formula. Albach [18] gave the exact solution of proximity effect losses under arbitrary field distribution, which needs to solve the exact external field distribution on each conductor's surface. Ewald and Biela [19], [20] derived field strength inside the core window of gapped inductors and calculated winding losses based on spatial r.m.s. field strength on a layer. Besides, several empirical equations are proposed with the help of FEM. Nan and Sullivan [7], [21] proposed a semiempirical equation to improve proximity effect estimation. Dimitrakakis et al. [22] proposed a semiempirical model for winding with arbitrary conductors distribution. Bahmani et al. [23] proposed a pseudo-empirical model for foil and round winding losses. Ahmed et al. [24] provided an air-core winding loss calculation model based on fitted field strength. The idea of homogenized complex permeability is used to facilitate loss calculation in FEM [25].

In this article, a revised Ferreira's formula is proposed for 1-D models. This revision is based on the relationship between fixed MMF across the core window and the frequency-dependent external field. Furthermore, a 2-D approach is proposed. Like many other approaches, skin and proximity effect losses are considered separately. The proximity effect losses are based on equivalent external fields, which take into account the changing magnetic field due to eddy currents. The method of images is used to obtain the dc magnetic field distribution. The rest of this article is organized as follows. Section II provides the revised 1-D formula and its theoretical derivation. Section III introduces

Manuscript received 5 July 2022; revised 16 September 2022 and 2 December 2022; accepted 15 December 2022. Date of publication 20 December 2022; date of current version 14 February 2023. This work was supported by China Scholarship Council under Grant 202007720032. Recommended for publication by Associate Editor Y. Siwakoti. *(Corresponding author: Tianming Luo.)*

Tianming Luo and Mohamad Ghaffarian Niasar are with the Electrical Sustainable Energy (ESE) Department, Delft University of Technology, 2628 CD Delft, The Netherlands (e-mail: t.luo-1@tudelft.nl; m.ghaffarianniasar@tudelft.nl).

Peter Vaessen is with the Electrical Sustainable Energy (ESE) Department, Delft University of Technology, 2628 CD Delft, The Netherlands, and also with the KEMA Laboratories, 6812 DE Arnhem, The Netherlands (e-mail: p.t.m.vaessen@tudelft.nl).

Color versions of one or more figures in this article are available at https://doi.org/10.1109/TPEL.2022.3230724.

Digital Object Identifier 10.1109/TPEL.2022.3230724

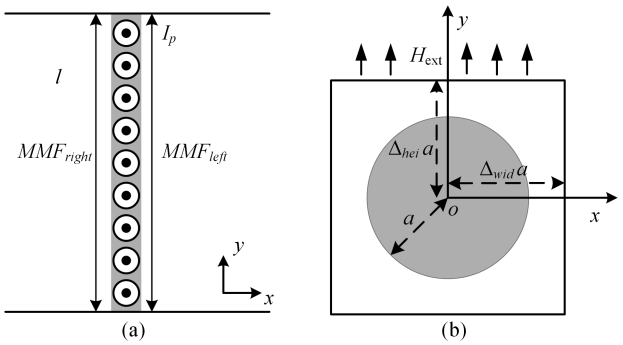

Fig. 1. (a) 1-D winding model composed of round conductors. (b) Conductor cell under a uniform external field.

the proposed 2-D winding resistance calculation approach based on the analytical solution and the method of images. Section IV compares the results from several different analytical methods, FEM simulations, and measurements. Finally, Section V concludes this article.

II. Revised 1-D Ferreira's Formula

The 1-D analytical method, i.e., Dowell's method and Ferreira's formulas, assumes a perfect core and windings that fully occupy the core window, like Fig. 1(a). Therefore, there is only a magnetic field component parallel to the winding layers. Because of the orthogonality between the skin and proximity effects [2], losses per unit length can be calculated by considering skin and proximity effect losses independently and summing them together. Ferreira's formulas are based on the analytical solution for skin effect in a single round conductor (1) and proximity effect in a single round conductor under a uniform sinusoidal external magnetic field (2) [26], [27].

$$\begin{aligned} P_{skin} &= \frac{1}{2} F_{ac} R_{dc} I_p^2 \\ F_{ac} &= \frac{1}{2}\left(\frac{J_0(\zeta_1)}{J_0(\zeta_1)+J_2(\zeta_1)}+\frac{J_0(\zeta_2)}{J_0(\zeta_2)+J_2(\zeta_2)}\right) \end{aligned} \tag{1}$$

$$\begin{aligned} P_{proxi} &= \frac{1}{2} G_{ext} H_{ext}^2 \\ G_{ext} &= j\pi a^2 \omega \mu_0 \left(\frac{J_2(\zeta_2)}{J_0(\zeta_2)}-\frac{J_2(\zeta_1)}{J_0(\zeta_1)}\right) \end{aligned} \tag{2}$$

where I_p and H_{ext} are the peak value of the current and the external magnetic field applied to the conductor, a, σ are the radius and the conductivity of the conductor, ω is the angular frequency, μ_0 is the vacuum permeability, and J_0 and J_2 are the zero and second-order Bessel functions of the first kind, respectively, $\zeta_1 = (1+j)\ a/\delta$, $\zeta_2 = (1-j)\ a/\delta$ where $\delta = \sqrt{2/\omega\mu_0\sigma}$ is the skin depth.

Although Ferreira's formulas are derived from the exact analytical solution for round conductors, they lead to considerable overestimation for compacted windings, as aforementioned. One important reason is the miscalculation of the H_{ext}. The H_{ext} of the mth layer is generally calculated from the average of both sides' MMF across the core window of the mth layer, as (3). l is the height of the core window.

$$H_{ext} = \frac{MMF_{rigth} + MMF_{left}}{2l}. \tag{3}$$

According to [26], for a case like Fig. 1(b), if the H_{ext} is along the y-direction, the magnetic field strength along y-direction outside the conductor can be easily derived

$$H_y = H_{ext} - \frac{a^2 H_{ext} J_2(\zeta_2)}{J_0(\zeta_2)} \frac{\left(x^2-y^2\right)}{\left(x^2+y^2\right)^2}. \tag{4}$$

It can be seen from (4) that the induced eddy current influences the magnetic field strength near the conductors, and only when the point is infinite far from the conductor the field strength can be regarded as H_{ext}. Therefore, it is unreasonable to obtain H_{ext} from (3) because the MMFs is a constant value at each side of a conductor layer, which cannot be regarded as infinite far.

Next, the correct relation between MMFs and H_{ext} needs to be found. Under the 1-D model's assumption, conductors in the mth layer can be regarded as infinite repeated cells, like Fig. 1(b). Because the y-axis is the even symmetry axis, the relation between MMF and H_{ext} can be obtained by integrating H_y over one of the vertical edge of cell, which is equal to the MMF.

$$\begin{aligned} \frac{MMF}{n} &= 2a\Delta_{hei} H_{ave} = \int_{-\Delta_{hei}a}^{\Delta_{hei}a} H_y dy \\ &= 2a\Delta_{hei} H_{ext}\left(1-\frac{J_2(\zeta_2)}{J_0(\zeta_2)\left(\Delta_{hei}^2+\Delta_{wid}^2\right)}\right). \end{aligned} \tag{5}$$

The Δ_{hei} can be easily determined by the core window height l and the number of turns n in this layer. The Δ_{wid} is just set as 1 to make sure the distorted magnetic field is mainly caused by the eddy current in the nearest conductor. To mark the different physical meanings of field strength from (3), H_{ave} is obtained from (3) instead of H_{ext}. According to the relation between H_{ave} and H_{ext} in (5), (2) becomes

$$\begin{aligned} P_{proxi} &= \frac{1}{2} G_{ave} H_{ave}^2 \\ G_{ave} &= j\pi a^2 \omega \mu_0 \left(\frac{J_2(\zeta_2)}{J_0(\zeta_2)-\frac{J_2(\zeta_2)}{1+\Delta_{hei}^2}}-\frac{J_2(\zeta_1)}{J_0(\zeta_1)-\frac{J_2(\zeta_1)}{1+\Delta_{hei}^2}}\right). \end{aligned} \tag{6}$$

Then, the total losses per unit length of the mth layer are as follows:

$$P_m = \tfrac{1}{2} I_p^2 \left(n F_{ac} R_{dc} + \frac{(2m-1)^2 n^2}{4l^2} G_{ave}\right). \tag{7}$$

The revised 1-D Ferreira's formulas (7) solve the mismatch between the external magnetic field and the magnetic field parallel to the winding layers. However, they still do not fully solve the interaction between different conductors' eddy current, which is distance related, and the proximity effect caused by conductors in the same layer. The comparison between the original and revised formulas is shown in Section IV.

In actual situations, the 1-D models only can be applied to limited winding layouts. There are a large number of winding configurations that do not comply with the 1-D assumption.

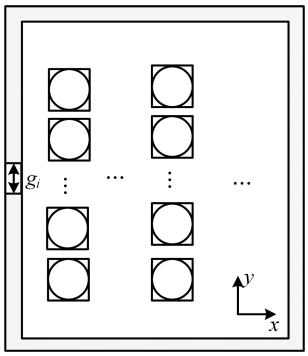

Fig. 2. Diagram for 2-D winding configuration.

Therefore, a 2-D winding loss calculation approach is proposed in the next section.

III. 2-D Winding Losses Calculation

There could be air gaps in magnetic cores, or winding layers do not fill the entire core window. In such cases, the one-direction magnetic field assumption in the 1-D model cannot be fulfilled, like the configuration in Fig. 2. Under these cases, a 2-D model is a better choice.

The proposed 2-D winding losses calculation approach is based on the analytical solution used in Ferreira's formula. It calculates the equivalent external field by iteratively calculating the eddy current induced field until a convergent point is reached. The skin and proximity effect losses are still considered independently in the approach. For the skin effect losses, (1) is used for each conductor. For the proximity effect losses, the losses under arbitrary field distribution are calculated by summing losses caused by x- and y-direction equivalent external fields.

The equivalent external field is based on each conductor cell, whose Δ_{hei} and Δ_{wid} are set as 1. There are two options to obtain the external magnetic field, one is to use the field strength on two edges parallel to the external magnetic field, and another is to use the field strength on all four edges of a cell. With the first option, H_{ext} can be obtained from (8), which works for both x- and y-direction external fields. $\overline{H_p}$ is the average of the magnetic field along the two parallel edges and calculated by summing each conductor's contribution.

$$H_{ext} = \frac{\overline{H_p} * J_0(\zeta_2)}{J_0(\zeta_2) - J_2(\zeta_2)/2}. \tag{8}$$

For the second option, calculate the average magnetic field on all four edges using (4) and (9), which are field strength distributions along the external field direction. H_{ext} along x- or y-direction can be obtained from the corresponding average field strength (10). $\overline{H_{all}}$ is also calculated by summing each conductor's contribution.

$$H_x = H_{ext\_x} + \frac{a^2 H_{ext\_x} J_2(\zeta_2)}{J_0(\zeta_2)} \frac{(x^2 - y^2)}{(x^2 + y^2)^2} \tag{9}$$

$$H_{ext} = \overline{H_{all}}\,. \tag{10}$$

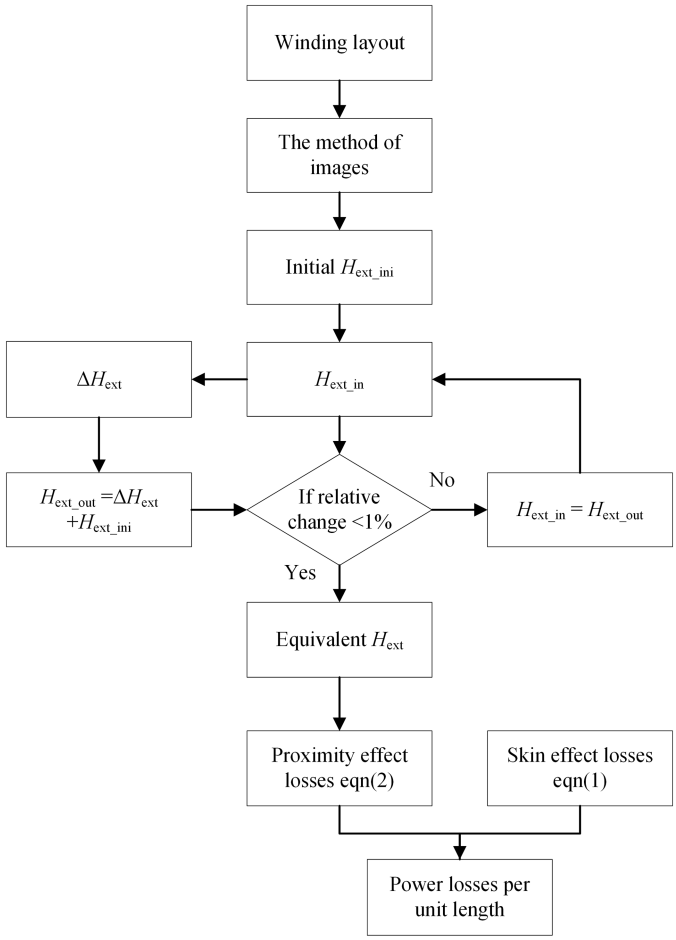

Fig. 3. Flowchart for proposed 2-D winding losses approach.

Here, the mean value of two options is used because the first option would underestimate the distance-related eddy current impact from adjacent conductors. For example, when calculating the contribution from a close conductor, the changing field value caused by the conductor is not uniform over the targeted conductor and is heavier on the closer edges. The second option would overestimate this impact. Therefore, the average value is used.

Fig. 3 shows the procedure to determine the equivalent uniform external fields. The method of images is used to replace the effect of a magnetic boundary [13], [28], as shown in Fig. 4(a). The current in the image conductor is the real current multiplied by the image coefficient k_i, which is defined as [29]. Each real and image conductor forms a cell. After forming cells, the magnetic field under the dc situation is set as the initial equivalent external magnetic field in iteration.

$$k_i = \frac{\mu_r - 1}{\mu_r + 1}. \tag{11}$$

For simplification, the magnetic core is assumed to be ideal, so $k_i = 1$. The internal reflection due to the finite thickness of the core is negligible under certain situations, which is assumed to be fulfilled [30]. Fig. 4(b) shows the method of images for

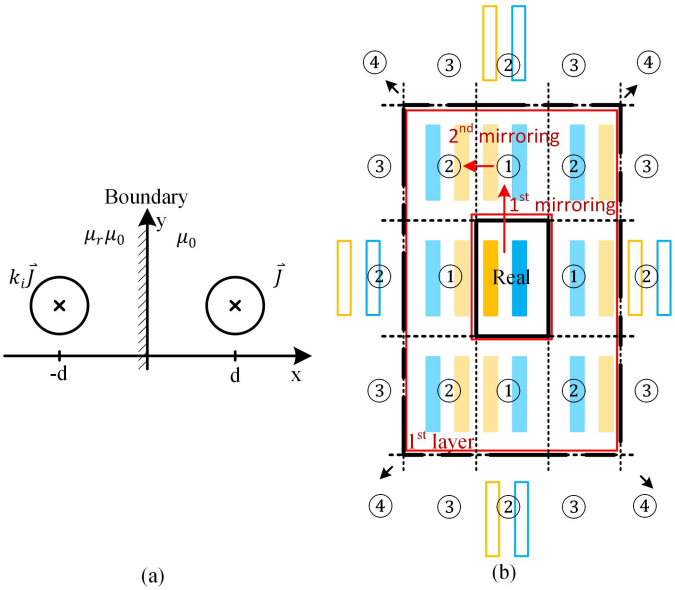

Fig. 4. Illustration of the method of images, (a) basic idea, (b) method applied to a core window, the number in a circle marks the required times of mirroring.

cases inside the core window. Generally, for cases inside the core window, the number of layers of images is used to count the images, like the enclosed first layer of images by the rectangles. However, in this article, the times of mirroring are used to build the images. The number in a circle marks the required times of mirroring to form these images. For example, it needs to mirror the real windings once to form the images marked by ①. Compared with using the number of layers, the times of mirroring can provide more accurate dc field results in some cases, as shown in Section IV-B. The N represents the number of layers or the times of mirroring.

If there is an air gap, a counter MMF source is placed at the air gap [13], [31]. The counter MMF source is represented by a surface current determined in (12), g is the air gap's height. The surface current also follows the method of images. However, when the location is very close to the gap, the field calculated by the MMF source may have considerable error. Roshen derived fringing field formulas due to an air gap, which can be used to calculate the field [32], [33]. To check the accuracy of the field strength calculation, the field on the left edge of the middle cell in the first layer in Case 1, which is the closest edge to the gap, is calculated and shown in Fig. 5. Both results are comparable with FEM's results. Therefore, the MMF source is used to calculate field strength caused by fringe flux.

$$J = -\sum I/g. \tag{12}$$

The $\overline{H_x}$ and $\overline{H_y}$ on one cell's edges generated by a conductor are calculated in (13) and (14), respectively. x_i and y_i are target point's coordinates, x_j and y_j are source conductor center's coordinates. Then, sum together all conductor's contributions to one cell, which is the initial value.

$$\overline{H_x} = -\frac{I}{2\pi l}\int_l \frac{y_{ij}}{x_{ij}^2+y_{ij}^2}dl \tag{13}$$

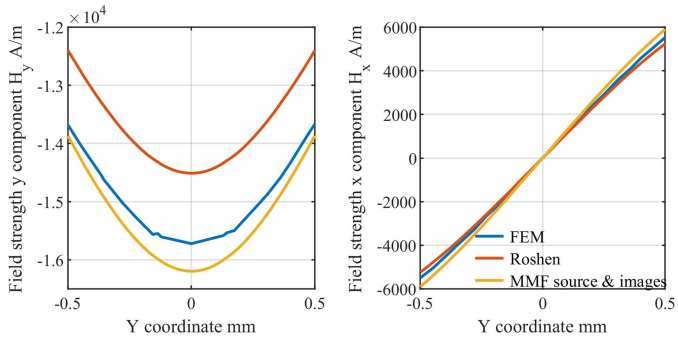

Fig. 5. Field strength calculated by different methods on the left edge of the middle cell in the first layer for Case 1.

$$\overline{H_y} = \frac{I}{2\pi l}\int_l \frac{x_{ij}}{x_{ij}^2+y_{ij}^2}dl \tag{14}$$

$$x_{ij} = x_i - x_j$$

$$y_{ij} = y_i - y_j. \tag{15}$$

After obtaining the initial value H_{ext_ini}, which is set as the input field value H_{ext_in} for the first loop, the magnetic field changes due to eddy current ΔH_{ext} are calculated, and the changing part caused by H_{ext_x} induced eddy current from (9) is

$$\begin{aligned} H_{x\_x} &= \frac{a^2 H_{extx} J_2(\zeta_2)}{J_0(\zeta_2)} \frac{x_{ij}^2-y_{ij}^2}{\left(x_{ij}^2+y_{ij}^2\right)^2} \\ H_{y\_x} &= \frac{a^2 H_{extx} J_2(\zeta_2)}{J_0(\zeta_2)} \frac{2x_{ij}y_{ij}}{\left(x_{ij}^2+y_{ij}^2\right)^2} \end{aligned}. \tag{16}$$

The changing due to H_{ext_y} induced eddy current from (4) is

$$\begin{aligned} H_{y\_y} &= \frac{a^2 H_{exty} J_2(\zeta_2)}{J_0(\zeta_2)} \frac{y_{ij}^2-x_{ij}^2}{\left(x_{ij}^2+y_{ij}^2\right)^2} \\ H_{x\_y} &= \frac{a^2 H_{exty} J_2(\zeta_2)}{J_0(\zeta_2)} \frac{2x_{ij}y_{ij}}{\left(x_{ij}^2+y_{ij}^2\right)^2} \end{aligned}. \tag{17}$$

Equations (16) and (17) can calculate the changing field on each cell due to other conductors. The output value H_{ext_out} is obtained by summing the initial value H_{ext_ini} and changing part ΔH_{ext}. The output value becomes the input value for the next loop. Repeat this loop until the relative change between the summation of all cells' input and output equivalent field squared is smaller than a threshold value, and 1% is used. The reason to use the summation of field squared as the index is that proximity loss is proportional to field squared.

Finally, use the iteration results and (2) to calculate the proximity effect losses. Sum all real conductors' losses to obtain the winding losses per unit length and scale the losses to get an estimated value.

The preceding approach is based on sinusoidal currents, but non-sinusoidal currents are normal in power electronics. For nonsinusoidal currents, the winding losses caused by each harmonic component can be calculated separately and added because of linearity. The amplitude of each harmonic can be obtained by Fourier transformation. Then, the summation of harmonics gives the total winding loss.

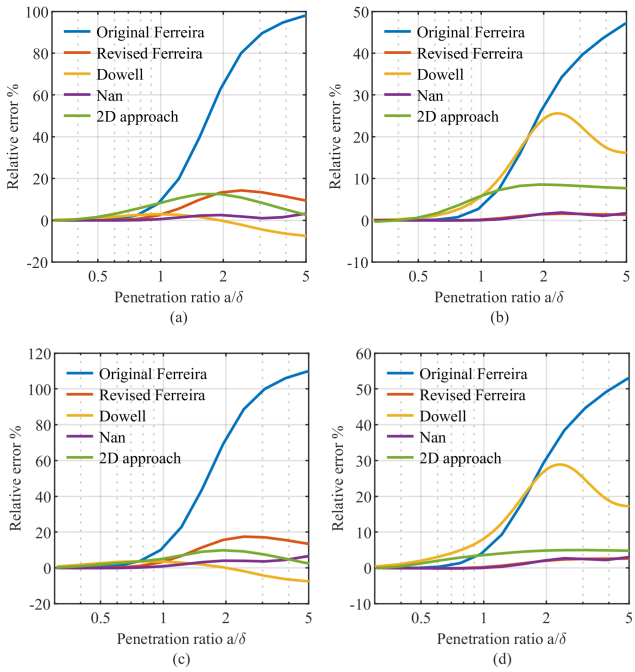

Fig. 6. Relative difference in % between different equations and 2-D FEM with varying layouts of layer. (a) Second layer with $\Delta_{hei} = \Delta_{wid} = 1.1$. (b) Second layer with $\Delta_{hei} = \Delta_{wid} = 1.6$. (c) Fourth layer with $\Delta_{hei} = \Delta_{wid} = 1.1$. (d) Fourth layer with $\Delta_{hei} = \Delta_{wid} = 1.6$.

IV. Simulation and Measurement

This section compares estimated values from different approaches to 2-D FEM results. 2-D FEM is done with commercial software COMSOL.

A. 1-D Windings

A 1-D model can be used as described in Section II when the assumptions are fulfilled of a perfect core and windings fully occupy the core window. A winding layer is composed of several round conductors with the same Δ_{hei} and Δ_{wid}. This section compares the total losses per unit length of a layer from different analytical equations and FEM.

Fig. 6 show the relative error of different equations of the second and fourth layer compared with 2-D FEM with two different layer setting. Revised Ferreira's formula improves the accuracy significantly compared with the original one. From (a) and (c), the revised formula would overestimate the losses by 10% to 20% when a/δ is higher than 1.5. Because it does not fully solve the interaction between different conductors' eddy currents, which has more impact when Δ_{hei} is small. The Dowell model would overestimate the losses when Δ_{hei} is large, i.e., sparse windings. Results from the 2-D approach do not show better results than others, but its maximal relative error stays around 10% for all cases. Nan's equation [20] shows the most stable and accurate result for 1-D cases among the five used equations.

Although revised Ferreira's formula does not provide the most accurate result, it significantly improves the accuracy compared with the original one because it solves the neglect of interaction between conductors to some degree.

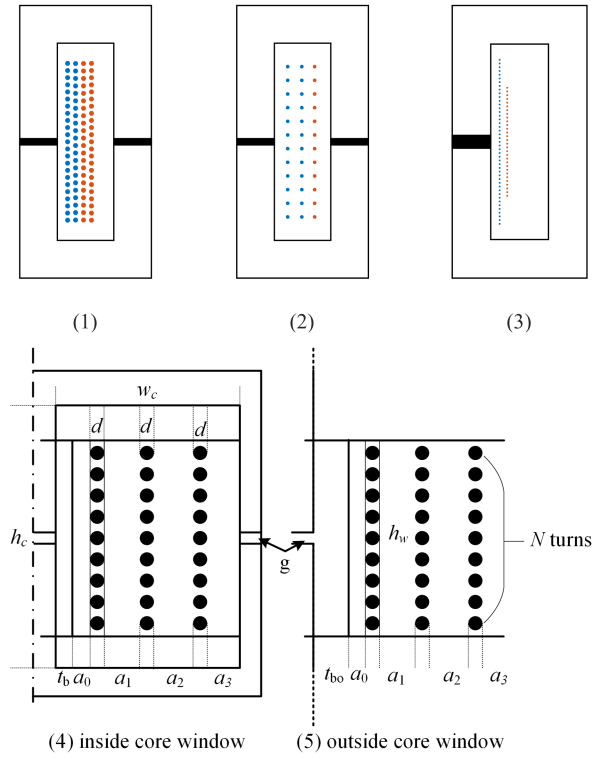

Fig. 7. Illustration of winding configurations, (1) and (2) equal layer winding heights with different Δ_{hei} and Δ_{wid}, (3) different layer winding heights. Notation of windings inside the core window (4) and outside the core window (5).

TABLE I
Detail Information About Winding Configurations

Sample	Case 1	Case 2	Case 3
Conductor diameter d [mm]	1	0.8	0.5
Number of turns n_*	[23,22;22,23]	[12,12;12]	[45;30]
Height of winding h_w [mm]	26.1	26.1	26.1;17.4
Parameter a_* [mm]	[0.04, 0.27, 0.27, 0.27, 3.05]	[0.625, 1.45, 1.45, 1.98]	[0.04, 0.68, 6.18]
Thickness of bobbin t_b/t_{bo} [mm]	1.1/1.75	1.1/1.75	1.1/1.1
Air gap g_i for inductor [mm]	1	1	2 (only on the left leg)
Height of core window h_c [mm]	$30.4 + g_i$	$30.4 + g_i$	30.4
Width of the core window w_c [mm]	9	9	9

B. 2-D Windings

Compared with 1-D cases, a 2-D model is more practicable for common cases. This section shows the cases with three different winding configurations with and without air gap cores, as shown in Fig. 7. Black parts are possible air gaps, and conductors with the same color are of the same winding. Details about the configurations are in Table I. The semi-colon in the row "Number of turns" of Table I separates the information of two windings.

First, the resistance per unit length for the core window without air gap cores is calculated. Resistances per unit length are referred to the winding with more turns. In cases (1) and (2), windings have equal height but do not fill the core window

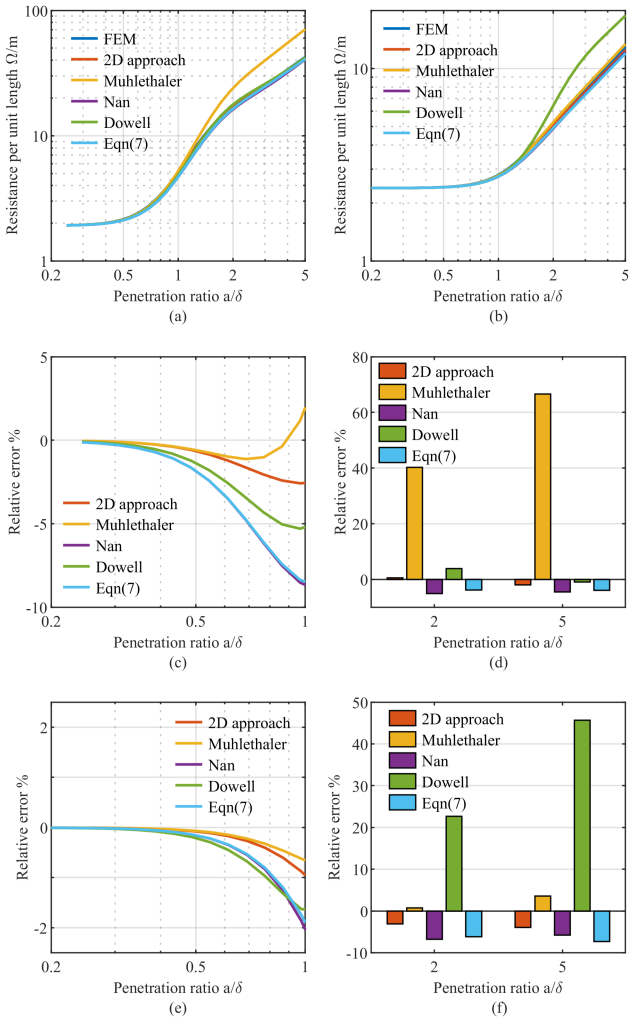

Fig. 8. Resistances per unit length and relative error compared with 2-D FEM in transformer mode without air gap, case (1), (a), (c), and (d), respectively. Case (2), (b), (e), and (f), respectively.

height, roughly 15% less. Two windings in a core window have opposite total MMF, like transformers. FEM, the proposed 2-D approach, Mühlethaler's approach, and three 1-D methods are used. For the 1-D methods, Δ_{hei} is determined by the number of turns and the core window's height, not the windings' height. The default times of mirroring are 2 to construct images.

Fig. 8(a), (c), and (d) show the result of case (1). All approaches or equations provide less than 10% error results when $a/\delta \leq 1$. The 2-D approach and Mühlethaler's approach have less error than other 1-D equations. However, Mühlethaler's approach has significant errors when the frequency is high, as shown in (d). For case (2), which has a larger Δ_{hei}, the 2-D approach and Mühlethaler's approach has better results. Dowell's method overestimates significantly at high frequency, and the other two 1-D methods underestimate less than 10%. It indicates that 15% shorter windings do not reduce the effectiveness of 1-D methods much. Case (3) has a different height of the winding, but the distance between turns is the same. For this case, two different settings are used. One is transformers mode, i.e., two winding have opposite total MMF. Another is

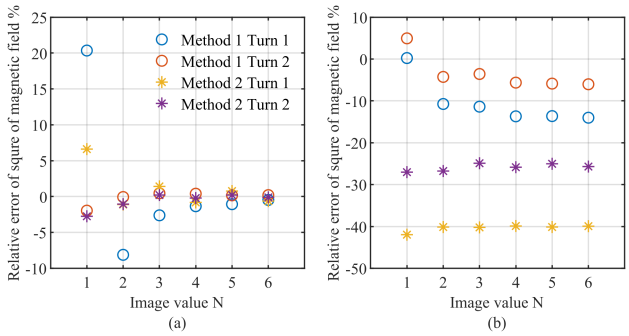

Fig. 9. Relative error of square of magnetic field compared with FEM results. (a) Transformer mode. (b) Inductor mode. Method 1 uses the times of mirroring. Method 2 uses the number of layers to count images. Turn 1 represents the top turn in first layer, and turn 2 represents the top turn in second layer.

inductor mode, i.e., each turn has the same current. Besides, the impact of different image settings is discussed. For case (3), each layer's top and bottom turns would contribute much higher eddy current losses due to the high field strength. The image setting would influence the initial value and impact the estimation of interaction between turns.

Fig. 9 shows the relative error of the square of the magnetic field of two top turns compared with the FEM result. In both methods, when the *N* is larger than 2, the results are stable. For transformer mode, the relative error is smaller than 10% when *N* is larger than 2. However, using the number of layers has significant errors in inductor mode. The results for both turns have more than 20% error even for *N* equal to 6. Therefore, it is better to use the times of mirroring to count images.

Fig. 10(a), (c), and (d) show the resistances per unit length and relative error compared with 2-D FEM in transformer mode. Only one 1-D method, i.e., revised Ferreira's formula, is used. It is obvious that 1-D methods do not suit this kind of case. They ignore the losses caused by another direction magnetic field, which is considerable in this case. Both the proposed 2-D approach and Mühlethaler's approach give accurate estimation when $a/\delta < 2$. For higher a/δ, the proposed 2-D approach has better accuracy. Besides, results with different image setting values are compared. When value *N* changes from 1 to 2, the relative error slightly decreases, and the change is not obvious when N increases again.

Fig. 10(b), (e), and (f) show the results of inductor mode. Mühlethaler's approach has a similar performance as the 2-D approach when $a/\delta \leq 1$. But it underestimates the resistance considerably with higher frequency. Results from different methods for counting image show huge differences in this case. The result with one layer of images has poor accuracy. On the contrary, results using the times of mirroring have less than 10% error. Because the difference in the initial field value shown in Fig. 9. According to the changes due to various *N* values, the default value of *N* is set as 2. The higher *N* leads to longer computational time and little improved accuracy.

In all cases without an air gap, the proposed 2-D approach provides an accurate estimation with less than 10% error compared with 2-D FEM.

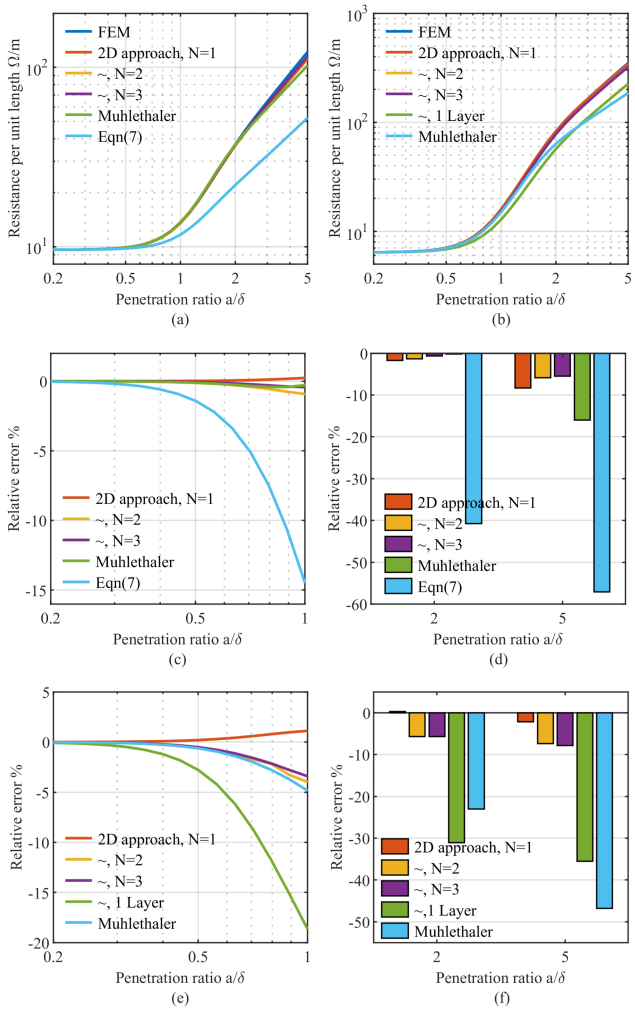

Fig. 10. Resistances per unit length and relative error compared with 2-D FEM in case (3) without air gap. Transformer mode, (a), (c), and (d), respectively. Inductor mode, (b), (e), and (f), respectively.

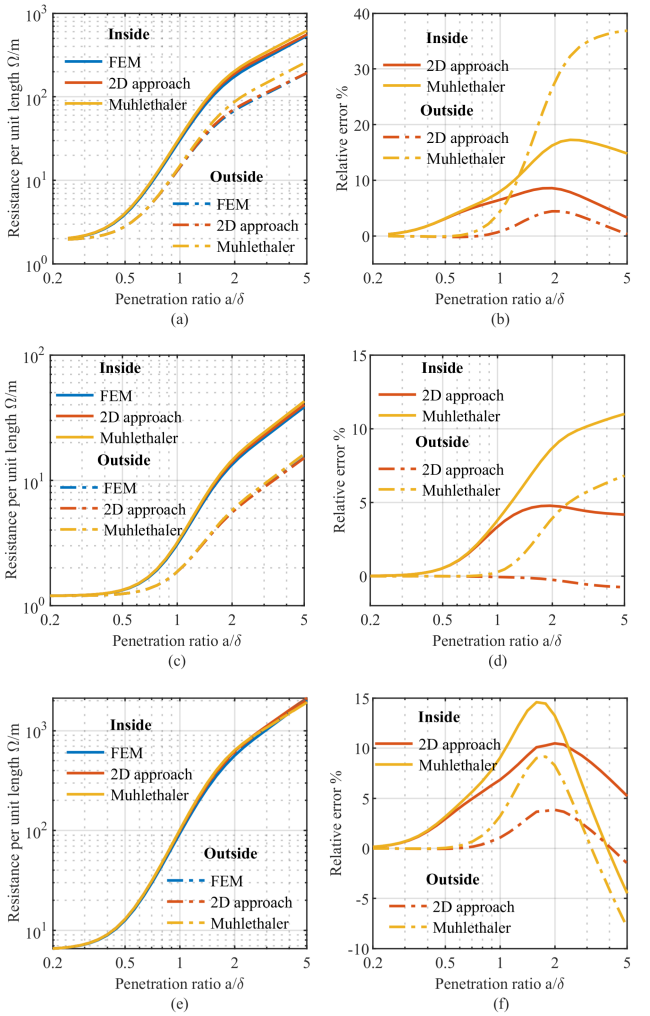

Fig. 11. Resistances per unit length and relative error compared with 2-D FEM in inductor cases. Case (1), (a) and (b). Case (2), (c) and (d). Case (3), (e) and (f), respectively.

Then, the resistance per unit length for the core window with air gap is calculated. All conductors in Fig. 7 are in the same winding, and air gaps are applied. Besides the resistances per unit length inside the core window, resistances outside the core window are also calculated for the double 2-D method [13], [34], [35], [36]. It needs to be mentioned that the air gap in 2-D FEM outside the core window is replaced by a magnetic core with a surface current density, which is determined in (11). The reason for making this substitution is that the flux density in the air gap is much smaller than inside the core window if the air domain is assigned to the air gap. This substitution leads to less than 10% overestimation for losses inside the core window. It is assumed that the substitution does not lead to a worse estimation for losses outside the core window.

Fig. 11 shows resistances per unit length and relative losses inside and outside the core window. For cases (1) and (2), the resistances per unit length inside and outside the core window significantly differ. Therefore, the double 2-D method is preferred. The proposed 2-D approach's estimations are close to 2-D FEM results. Mühlethaler's approach performs better in case (2) than in case (1) because it does not consider the interactions between eddy currents, and the distance between conductors is larger in case (2). In case (3), resistances per unit length inside and outside the core window do not show much difference because there is only one air gap. The proposed approach behaves better, with roughly 5% less highest error than Mühlethaler's approach for $a/\delta \leq 2$.

For inductor cases, both the proposed 2-D approach and Mühlethaler's approach give accurate estimations when $a/\delta \leq 1$. The proposed 2-D approach behaves more stable and accurately for the higher frequency region, which is good for applications with high harmonic distortion.

According to the 2-D winding resistance per unit length calculation, Mühlethaler's approach considers the initial magnetic field distribution and performs well when there is a dominant eddy current loss contributor, like fringe flux or a large magnetic field at the end of windings. Therefore, it has good accuracy for $a/\delta \leq 1$, even though it does not consider the interactions between eddy currents. Several 1-D methods would be effective when the windings have the same height and are not much shorter

TABLE II
COMPUTATIONAL TIME WITH 41 FREQUENCY POINTS

Sample	Case 1	Case 2	Case 3
FEM	90 s	46 s	71 s
Proposed 2D without gap, N=2	19.46 s	3.3 s	14.96 s
Proposed 2D with a gap, N=2	16.25 s	2.86 s	14.02 s
Inside/outside core window	/1.01 s	/0.26 s	/0.81 s

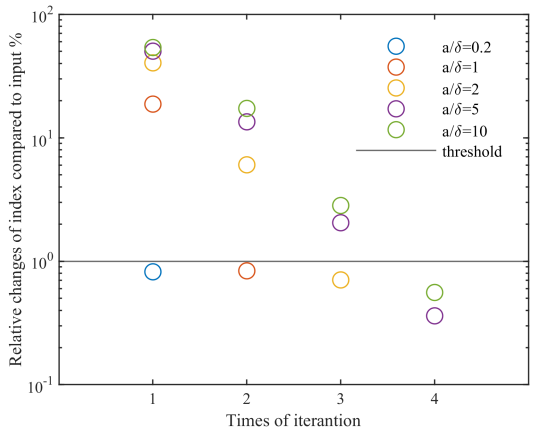

Fig. 12. Relative changes of the index in Case 1 without gap, $N = 2$.

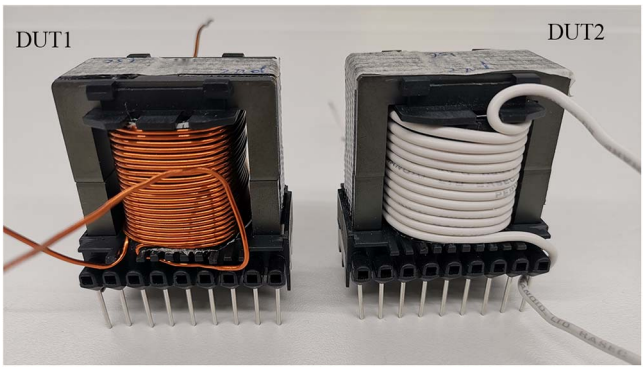

Fig. 13. Photograph of samples in transformer mode, left is the case (1), and right is the case (2).

than the core window height. The proposed 2-D approach is stable and accurate in most situations.

Another critical feature is computational time. Table II provides the computational time under different cases for the same computer. Each case's FEM uses the same mesh and has a similar computational time, which is much longer than the 2-D approach. The computational time for the outside core window is much shorter than the inside core window because of the smaller amount of image conductors.

Total computational time shows the multiplication of time used for an iteration and the number of iterations. Fig. 12 shows the relative changes of the index in Case 1 without a gap, which takes the longest time. For $a/\delta \leq 2$, it needs three iterations to reach the threshold.

TABLE III
DETAIL INFORMATION ABOUT SAMPLES

Sample	Case 1	Case 2
Core size	EE 42/21/20	
Core material	N87	
Effective magnetic length l_e [mm]	97	
Effective magnetic cross-section A_e [mm^2]	234	
Bobbin	B66243B1018T001	
Bobbin size $e \times f$ [mm]	23.5 × 14.2	
Mean turn length l_m [mm]	90.76	95.97
Partial length inside the core window l_{in} [mm]	40	40
Partial length outside the core window l_{out} [mm]	50.76	55.97

C. Measurement

In the preceding part, comparisons are made for 2-D windings. It is also needed to validate the results for real cases. Two windings, i.e., cases (1) and (2), were built on bobbins, as shown in Fig. 13. Details of the samples are shown in Table III. Two windings become primary and secondary windings, respectively, when measured as transformers, and one winding when measured as inductors.

An impedance analyzer Agilent 4294A was used for measurements. For transformers, the short circuit method was used. The secondary winding was shorted, and the two connections of the primary winding were connected to the impedance analyzer. The core losses are assumed ignorable. The resonant frequency is in the region $a/\delta > 15$, far from the interested region $a/\delta < 5$, and the measured ac resistance does not need correction.

Core losses are not negligible for inductors, and they can be modeled based on complex permeability or the Steinmetz equation [19], [37], [38]. Steinmetz factors are valid for a limited frequency and flux density range, and TDK N87 ferrite's datasheet does not provide factors with that low flux density. The complex permeability is available for small signal measurement. However, this method has some disadvantages. The complex permeability measurement is performed on a different sample, and the exact flux density is unclear. It may lead to less accurate R_c. Therefore, an auxiliary transformer with 2:2 turns windings was built to measure the core loss under the small signal. The conductor used 60-μm thickness copper tape to avoid the impact of eddy current in conductors. Two-winding method is used for core losses measurement. The parallel circuit is used to represent the measured core. The series core resistance can be obtained in (18) [39], where N_{DUT} is the inductors' turn number, N_{aux} is auxiliary transformer's turn number, i.e., 2, G_{aux} is measured parallel conductance and L is the inductor of two samples. The inductance L is determined by measured impedance at low frequency and is assumed constant.

$$R_c = \frac{(N_{DUT}/N_{aux})^2 G_{aux} \omega^2 L^2}{(N_{DUT}/N_{aux})^4 + \omega^2 L^2 G_{aux}^2}. \tag{18}$$

Despite core losses, the impact of parasitic capacitance C_p needs attention. An equivalent circuit of inductors, as shown in Fig. 14, is used to convert the measured ESR R_m to the summation of winding resistance R_w and core resistance R_c. The parasitic capacitance C_p is obtained by finding the inductors'

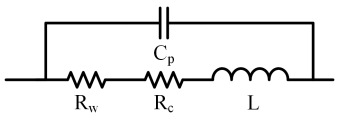

Fig. 14. Equivalent circuit of inductors.

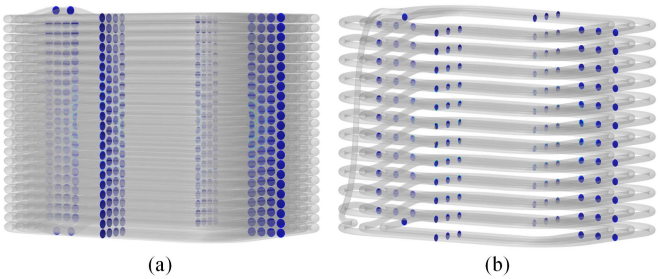

Fig. 15. Current density in the windings at $a/\delta = 4$ from 3-D FEM inductor mode. Case (1), (a). Case (2), (b).

self-resonant frequency and using the following equation:

$$C_p = \frac{1}{\omega_{res}^2 L}. \tag{19}$$

Then, the summation of R_w and R_c can be obtained in (20). The winding resistance is obtained in (18) and (20).

$$R_w + R_c = \frac{1 - \sqrt{1 - 4\omega^2 C_p^2 R_m^2 (1 - \omega^2 L C_p)^2}}{2\omega^2 C_p^2 R_m}. \tag{20}$$

In addition to the resistance correction, 3-D FEMs for two samples in both transformer and inductor modes were done to obtain the winding resistances. The simulations were computed with 16 cores and 500 GB memory [40]. To guarantee the accuracy of computation, the boundary layer mesh is used, and the smallest size of an element is smaller than one-third of skin depth based on analysis in [41]. The 3-D models have 2.6 million elements in case (1) and 1.6 million elements in case (2).

Fig. 15 shows the current density in the two inductor mode cases with $a/\delta = 4$. The turns near the air gaps have larger eddy current than others.

The resistances per unit length from the 2-D FEM and the proposed 2-D approach need to be scaled. Generally, the resistance per unit length is scaled by the mean turn length (MTL) l_m. However, the values inside and outside the core window differ significantly for inductors. Therefore, transformers use normal MTL, and inductors use the double 2-D method. The scaled methods are introduced in the Appendix.

The resistance of transformers from the measurement and the scaled values are shown in Fig. 16. In both cases, 3-D FEM results are close to measurement, and scaled resistance by 2-D FEM and 2-D approach follow the measured curves with less than 10% error. The relative error plots show the ac resistance factor, i.e., the ratio of ac resistance to dc resistance is well estimated through 2-D models. Nan's formula is used to compare with measurements representing the 1-D models. It also has less than 10% error, but it has more fluctuation, especially in case

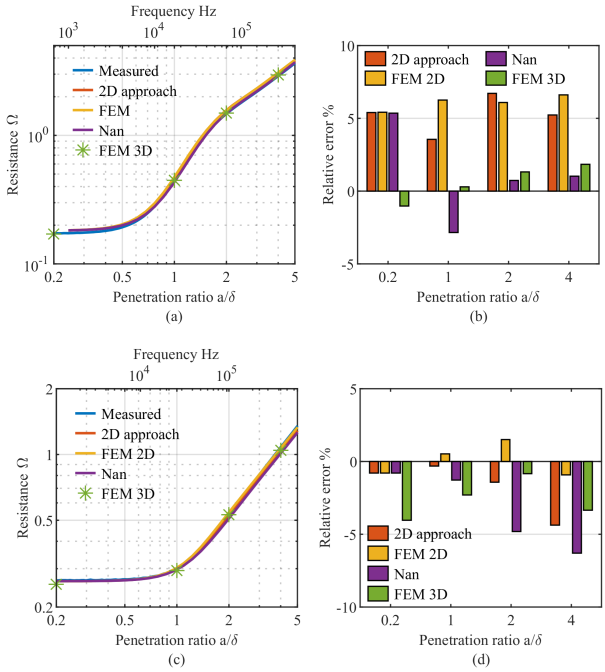

Fig. 16. Measured and scaled resistance and relative differences for transformers. Case (1), (a) and (b), respectively. Case (2), (c) and (d), respectively.

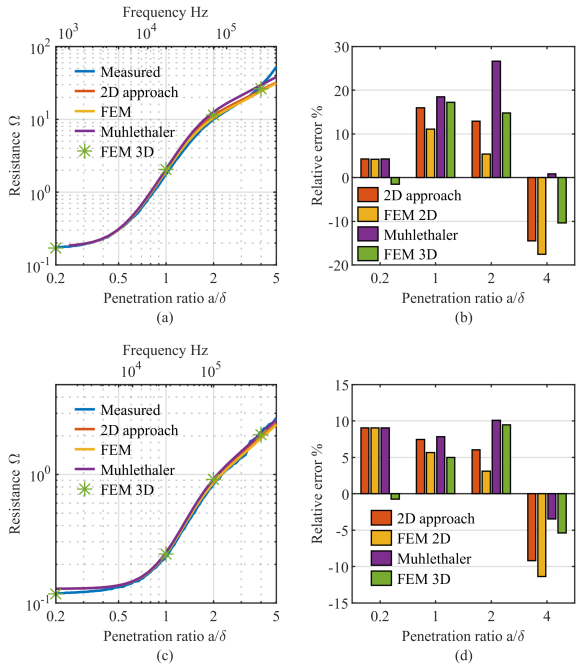

Fig. 17. Measured and scaled resistance and relative differences for inductors. Case (1), (a) and (b), respectively. Case (2), (c) and (d), respectively.

(1) with $a/\delta \approx 1$. Two scaled curves are a bit deviate from the measured curve, which could attribute to the imperfect matching between samples and scaled models.

Fig. 17 shows the resistance of inductors from the measurement and the scaled value. Compared with transformers' results, inductors' estimations obviously bigger difference from measurement, including 3-D FEM. For case (1), estimations

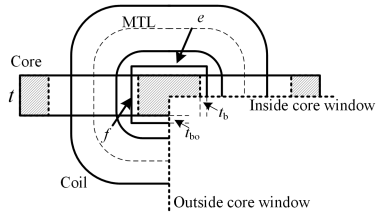

Fig. 18. Illustration of MTL calculation.

from the 2-D approach, 2-D and 3-D FEM have a similar trend. They overestimate the resistance when $a/\delta < 2$. Mühlethaler's approach has larger maximal error, which is over 20%. For case (2), all estimations have roughly less than 10% relative error compared with measurement. In both cases, 3-D FEM results match 2-D estimations better than measurement.

The difference between measurement and estimation could attribute to several aspects. The first aspect can be the resonant correction. When the testing frequency is near the resonant frequency, the results are very sensitive to the resonant frequency value. For case (1), the measured resonant frequency is at 493.8 kHz and the point $a/\delta = 4$ is 270 kHz. Therefore, the small error in resonant frequency could lead to some difference in winding resistance. The second aspect is the core loss prediction. When the frequency exceeds hundreds of kilohertz, the core losses are comparable to winding losses. The error in the core losses prediction can cause relatively large differences in winding resistance. Besides, factors like imperfect geometric parameters and impedance phase measurement errors can also lead to winding resistance errors.

According to the preceding result, several points can be obtained. First, 1-D equations cannot handle the cases where both x and y field components are considerable. The proposed 2-D approach and Mühlethaler's approach can provide almost the same accurate estimation with $a/\delta \leq 0.5$ compared with 2-D FEM. When the frequency increases, the interaction between conductors gradually plays a more important role, and the difference between the two approaches becomes obvious. It occurs at $a/\delta \approx 0.7$ for cases (1) and (3), and ≈ 1 for case (2) because the conductors are more compact in cases (1) and (3). Therefore, the proposed 2-D approach is more beneficial for windings where both the x and y field components cause considerable losses, and the interaction between turns is important, i.e., compact arrangement and waveforms with high harmonic content. In general, the 2-D approach can estimate winding loss with less than 10% error compared with 2-D FEM in most cases, and the scaled resistances with double 2-D method match results from 3-D FEM.

V. Conclusion

This article proposes a revised Ferreira's formula for 1-D winding losses calculation, which significantly reduces the error of the original formula for compact windings. Also, a 2-D approach is proposed, and equivalent external magnetic fields are calculated based on dc field distribution and eddy current induced field changing for each conductor cell. For 2-D models, the proposed approach has less than 10% error in all seven settings compared with 2-D FEM and shows good effectiveness as a 2-D approach. Compared with measured results, scaled resistances show good accuracy in transformer samples. For inductor samples, it has good accuracy compared with 3-D FEM results. But it has a larger error compared with measured data. The 2-D approach can be beneficial for designing magnetic components with compact windings and high harmonic content.

Appendix

For 2-D approaches, the obtained resistance per unit length needs to be scaled to estimate the resistance of windings. Generally, the scale length is determined by the MTL l_m , like (21). The MTL in EE cores can be calculated according to (22).

$$l_m = 2(e+f) + \pi(2a_0 + a_1 \ldots a_{n_l-1} + n_l d) \tag{21}$$

where e and f are the edge lengths of the bobbin in EE cores, as shown in Fig. 18, and n_l is the number of layers.

$$R = R_{unit,\,in}\ l_m. \tag{22}$$

The double 2-D method scales the resistance per unit length inside and outside the core window with the corresponding partial lengths according to

$$R = R_{unit,\,in}\ l_{in} + R_{unit,out} l_{out}. \tag{23}$$

The partial lengths for the double 2-D method can be calculated as follows:

$$\begin{aligned} l_{in} &= 2t \\ l_{out} &= l_m - l_{in} \end{aligned} \tag{24}$$

where t is the thickness of the core, which is 20 mm for EE42/21/20.

References

[1] P. L. Dowell, "Effects of eddy currents in transformer windings," *Proc. Inst. Elect. Engineers*, vol. 113, no. 8, 1966, Art. no. 1387.
[2] J. A. Ferreira, "Improved analytical modeling of conductive losses in magnetic components," *IEEE Trans. Power Electron.*, vol. 9, no. 1, pp. 127–131, Jan. 1994.
[3] M. Kaymak, Z. Shen, and R. W. de Doncker, "Comparison of analytical methods for calculating the AC resistance and leakage inductance of medium-frequency transformers," in *Proc. IEEE 17th Workshop Control Model. Power Electron.*, 2016, pp. 1–8.
[4] G. S. Dimitrakakis and E. C. Tatakis, "Investigation of high frequency effects on layered coils," in *Proc. IEEE 13th Int. Power Electron. Motion Control Conf.*, 2008, pp. 1301–1308.
[5] A. Reatti and M. K. Kazimierczuk, "Comparison of various methods for calculating the AC resistance of inductors," *IEEE Trans. Magn.*, vol. 38, no. 3, pp. 1512–1518, May 2002.
[6] T. Luo, M. G. Niasar, and P. Vaessen, "Improved winding losses calculation based on Bessel functions," *IEEE Trans. Magn.*, 2022, to be published, doi: 10.1109/TMAG.2022.3221803.
[7] X. Nan and C. R. Sullivan, "An improved calculation of proximity-effect loss in high-frequency windings of round conductors," in *Proc. IEEE 34th Annu. Conf. Power Electron. Specialist*, 2003, vol. 2, pp. 853–860.
[8] M. Bartoli, N. Noferi, A. Reatti, and M. K. Kazimierczuk, "Modeling Litz-wire winding losses in high-frequency power inductors," in *Proc. IEEE PESC Rec. 27th Annu. Power Electron. Specialists Conf.*, 1996, vol. 2, pp. 1690–1696.
[9] C. R. Sullivan, "Optimal choice for number of strands in a Litz-wire transformer winding," *IEEE Trans. Power Electron.*, vol. 14, no. 2, pp. 283–291, Mar. 1999.

[10] H. Hamalainen, J. Pyrhonen, J. Nerg, and J. Talvitie, "AC resistance factor of Litz-wire windings used in low-voltage high-power generators," *IEEE Trans. Ind. Electron.*, vol. 61, no. 2, pp. 693–700, Feb. 2014.
[11] C. R. Sullivan and R. Y. Zhang, "Analytical model for effects of twisting on Litz-wire losses," in *Proc. IEEE 15th Workshop Control Model. Power Electron.*, 2014, pp. 1–10.
[12] F. Tourkhani and P. Viarouge, "Accurate analytical model of winding losses in round Litz wire windings," *IEEE Trans. Magn.*, vol. 37, no. 1, pp. 538–543, Jan. 2001.
[13] J. Mühlethaler, J. W. Kolar, and A. Ecklebe, "Loss modeling of inductive components employed in power electronic systems," in *Proc. IEEE 8th Int. Conf. Power Electron.-ECCE Asia*, 2011, pp. 945–952.
[14] R. P. Wojda and M. K. Kazimierczuk, "Winding resistance of Litz-wire and multi-strand inductors," *IET Power Electron.*, vol. 5, no. 2, 2012, Art. no. 257.
[15] D. Whitman and M. K. Kazimierczuk, "An analytical correction to Dowell's equation for inductor and transformer winding losses using cylindrical coordinates," *IEEE Trans. Power Electron.*, vol. 34, no. 11, pp. 10425–10432, Nov. 2019.
[16] R. P. Wojda and M. K. Kazimierczuk, "Analytical optimization of solid-round-wire windings," *IEEE Trans. Ind. Electron.*, vol. 60, no. 3, pp. 1033–1041, Mar. 2013.
[17] M. Bartoli, N. Noferi, A. Reatti, and M. K. Kazimierczuk, "Modelling winding losses in high-frequency power inductors," *J. Circuits, Syst., Comput.*, vol. 05, no. 04, pp. 607–626, Dec. 1995.
[18] M. Albach, "Two-dimensional calculation of winding losses in transformers," in *Proc. IEEE 31st Annu. Power Electron. Specialists Conf.*, 2000, vol. 3, pp. 1639–1644.
[19] T. Ewald and J. Biela, "Analytical winding loss and inductance models for gapped inductors with Litz or solid wires," *IEEE Trans. Power Electron.*, vol. 37, no. 12, pp. 15127–15139, Dec. 2022.
[20] T. Ewald and J. Biela, "Frequency-dependent inductance and winding loss model for gapped foil inductors," *IEEE Trans. Power Electron.*, vol. 37, no. 10, pp. 12370–12379, Oct. 2022.
[21] X. Nan and C. R. Sullivan, "Simplified high-accuracy calculation of eddy-current loss in round-wire windings," in *Proc. IEEE Annu. Power Electron. Specialists Conf.*, 2004, vol. 2, pp. 873–879.
[22] G. S. Dimitrakakis, E. C. Tatakis, and E. J. Rikos, "A semiempirical model to determine HF copper losses in magnetic components with nonlayered coils," *IEEE Trans. Power Electron.*, vol. 23, no. 6, pp. 2719–2728, Nov. 2008.
[23] M. A. Bahmani, T. Thiringer, and H. Ortega, "An accurate pseudoempirical model of winding loss calculation in HF foil and round conductors in switchmode magnetics," *IEEE Trans. Power Electron.*, vol. 29, no. 8, pp. 4231–4246, Aug. 2014.
[24] D. Ahmed, L. Wang, M. Wu, L. Mao, and X. Wang, "Two-dimensional winding loss analytical model for high-frequency multilayer air-core planar inductor," *IEEE Trans. Ind. Electron.*, vol. 69, no. 7, pp. 6794–6804, Jul. 2022.
[25] X. Nan and C. R. Sullivan, "An equivalent complex permeability model for Litz-wire windings," *IEEE Trans. Ind. Appl.*, vol. 45, no. 2, pp. 854–860, Mar./Apr. 2009.
[26] J. Lammeraner and M. Štafl, *Eddy Currents*. Boca Raton, FL, USA: CRC Press, 1966.
[27] C. Carretero, J. Acero, and R. Alonso, "TM-TE decomposition of power losses in multi-stranded Litz-wires used in electronic devices," *Prog. Electromagn. Res.*, vol. 123, pp. 83–103, 2012.
[28] M. Lambert, F. Sirois, M. Martinez-Duro, and J. Mahseredjian, "Analytical calculation of leakage inductance for low-frequency transformer modeling," *IEEE Trans. Power Del.*, vol. 28, no. 1, pp. 507–515, Jan. 2013.
[29] P. Hammond, "Electric and magnetic images," *Proc. IEE Part C: Monographs*, vol. 107, no. 12, 1960, Art. no. 306.
[30] X. Margueron, A. Besri, P. O. Jeannin, J. P. Keradec, and G. Parent, "Complete analytical calculation of static leakage parameters: A step toward HF transformer optimization," *IEEE Trans. Ind. Appl.*, vol. 46, no. 3, pp. 1055–1063, May/Jun. 2010.
[31] A. Van den Bossche and V. C. Valchev, *Inductors and Transformers for Power Electronics*. Boca Raton, Florida, USA: CRC Press, 2005.
[32] W. A. Roshen, "Fringing field formulas and winding loss due to an air gap," *IEEE Trans. Magn.*, vol. 43, no. 8, pp. 3387–3394, Aug. 2007.
[33] S. Mukherjee, Y. Gao, and D. Maksimovic, "Reduction of AC winding losses due to fringing-field effects in high-frequency inductors with orthogonal air gaps," *IEEE Trans. Power Electron.*, vol. 36, no. 1, pp. 815–828, Jan. 2021.
[34] R. Prieto, J. A. Cobos, O. Garcia, P. Alou, and J. Uceda, "Study of 3-D magnetic components by means of 'double 2-D' methodology," *IEEE Trans. Ind. Electron.*, vol. 50, no. 1, pp. 183–192, Feb. 2003.
[35] A. Fouineau, M. A. Raulet, B. Lefebvre, N. Burais, and F. Sixdenier, "Semi-analytical methods for calculation of leakage inductance and frequency-dependent resistance of windings in transformers," *IEEE Trans. Magn.*, vol. 54, no. 10, Oct. 2018, Art. no. 8400510.
[36] R. Schlesinger and J. Biela, "Comparison of analytical models of transformer leakage inductance: Accuracy versus computational effort," *IEEE Trans. Power Electron.*, vol. 36, no. 1, pp. 146–156, Jan. 2021.
[37] B. X. Foo, A. L. F. Stein, and C. R. Sullivan, "A step-by-step guide to extracting winding resistance from an impedance measurement," in *Proc. IEEE Appl. Power Electron. Conf. Expo.*, 2017, pp. 861–867.
[38] M. Kazimierczuk, *High-Frequency Magnetic Components*. Chichester, U.K.: Wiley, 2013.
[39] K. Niyomsatian, J. J. C. Gyselinck, and R. V. Sabariego, "Experimental extraction of winding resistance in Litz-wire transformers—influence of winding mutual resistance," *IEEE Trans. Power Electron.*, vol. 34, no. 7, pp. 6736–6746, Jul. 2019.
[40] "Delft high performance computing centre (DHPC), DelftBlue supercomputer (Phase 1)," 2022. [Online]. Available: https://www.tudelft.nl/dhpc/ark:/44463/DelftBluePhase1
[41] L. Taylor, X. Margueron, Y. Le Menach, and P. Le Moigne, "Numerical modelling of PCB planar inductors: Impact of 3-D modelling on high-frequency copper loss evaluation," *IET Power Electron.*, vol. 10, no. 14, pp. 1966–1974, Nov. 2017.

Tianming Luo (Student Member, IEEE) was born in Jinan, China, in 1993. He received the B.E. degree in electrical engineering and automation from Chongqing University, Chongqing, China, in 2015, and the M.Sc. degree in electrical engineering from China Electric Power Research Institute, Beijing, China, in 2018. He is currently working toward the Ph.D. degree in electrical engineering with High Voltage Technologies Group, Delft University of Technology, Delft, The Netherlands.

His research interests are multiphysic model of medium frequency power transformer and insulation performance under medium frequency.

Mohamad Ghaffarian Niasar was born in Tehran, Iran, in 1984. He received the M.Sc. degree in electrical engineering from Sharif University of Technology, Tehran, Iran, in 2008, and the Ph.D. degree in electrical engineering from Royal Institute of Technology, Stockholm, Sweden, in 2015.

He is currently an Assistant Professor with High Voltage Technologies Group, Delft University of Technology, Delft, The Netherlands. His main research interests are aging of insulation material, HVdc insulation system, high frequency power transformers, and multiphysics modeling of power components.

Peter Vaessen (Member, IEEE) was born in Maasbree, The Netherlands, in 1960. He received the M.Sc. degree (*cum laude*) in electrical power engineering from Eindhoven Technical University, Eindhoven, The Netherlands, in 1985,

In 1985, he joined KEMA (now a CESI brand). In his 35-year career, he held research positions in the field of large power transformers and high voltage measurement and testing. He has 25 years of experience in (U)HVdc technology and T&D grids with high shares of renewables. He is manager innovations with KEMA Laboratories and Chairman of the European Distributed Energy Resources Laboratories association (DERlab), as well as a Member of several national and international working groups. Since 2017, he has been a Part-Time Professor of Hybrid Transmission Systems with TU Delft, Delft, The Netherlands, where he teaches high voltage technology and HVdc.